This is the peer reviewd version of the followng article:

Surface engineering of Solid Lipid Nanoparticle assemblies by methyl α-d-mannopyranoside for the active targeting to macrophages in anti-tuberculosis inhalation therapy / Maretti, Eleonora; Costantino, Luca; Rustichelli, Cecilia; Leo, Eliana Grazia; Croce, Maria Antonietta; Francesca, Buttini; Truzzi, Eleonora; Iannuccelli, Valentina. - In: INTERNATIONAL JOURNAL OF PHARMACEUTICS. - ISSN 0378-5173. - 528:1-2(2017), pp. 440-451. [10.1016/j.ijpharm.2017.06.045]

Terms of use:

The terms and conditions for the reuse of this version of the manuscript are specified in the publishing policy. For all terms of use and more information see the publisher's website.

12/10/2024 04:55

(Article begins on next page)

Accepted Manuscript

Title: Surface engineering of Solid Lipid Nanoparticle assemblies by methyl α-D-mannopyranoside for the active targeting to macrophages in anti-tuberculosis inhalation therapy

Authors: Eleonora Maretti, Luca Costantino, Cecilia Rustichelli, Eliana Leo, Maria Antonietta Croce, Francesca Buttini, Eleonora Truzzi, Valentina Iannuccelli

PII: S0378-5173(17)30553-7
DOI: http://dx.doi.org/doi:10.1016/j.ijpharm.2017.06.045
Reference: IJP 16769

To appear in: *International Journal of Pharmaceutics*

Received date: 4-5-2017
Revised date: 6-6-2017
Accepted date: 13-6-2017

Please cite this article as: Maretti, Eleonora, Costantino, Luca, Rustichelli, Cecilia, Leo, Eliana, Croce, Maria Antonietta, Buttini, Francesca, Truzzi, Eleonora, Iannuccelli, Valentina, Surface engineering of Solid Lipid Nanoparticle assemblies by methyl α-d-mannopyranoside for the active targeting to macrophages in anti-tuberculosis inhalation therapy.International Journal of Pharmaceutics http://dx.doi.org/10.1016/j.ijpharm.2017.06.045

This is a PDF file of an unedited manuscript that has been accepted for publication. As a service to our customers we are providing this early version of the manuscript. The manuscript will undergo copyediting, typesetting, and review of the resulting proof before it is published in its final form. Please note that during the production process errors may be discovered which could affect the content, and all legal disclaimers that apply to the journal pertain.

ACCEPTED MANUSCRIPT

Surface engineering of Solid Lipid Nanoparticle assemblies by methyl α-D-mannopyranoside for the active targeting to macrophages in anti-tuberculosis inhalation therapy

Eleonora Maretti [a], Luca Costantino [a], Cecilia Rustichelli [a], Eliana Leo [a], Maria Antonietta Croce [a], Francesca Buttini [b], Eleonora Truzzi [a], Valentina Iannuccelli [a,*]

[a] Department of Life Sciences, University of Modena and Reggio Emilia, via G. Campi 103, 41125 Modena, Italy
[b] Department of Food and Drug Science, University of Parma, Parco Area delle Scienze 27/A, 43124 Parma, Italy

* Corresponding author:
Valentina Iannuccelli
Department of Life Sciences
University of Modena and Reggio Emilia
Via G. Campi 103, Modena, Italy
Phone: +39 059 2058559
Fax: +39 059 2055131
E-mail: valentina.iannuccelli@unimore.it

Graphical abstract

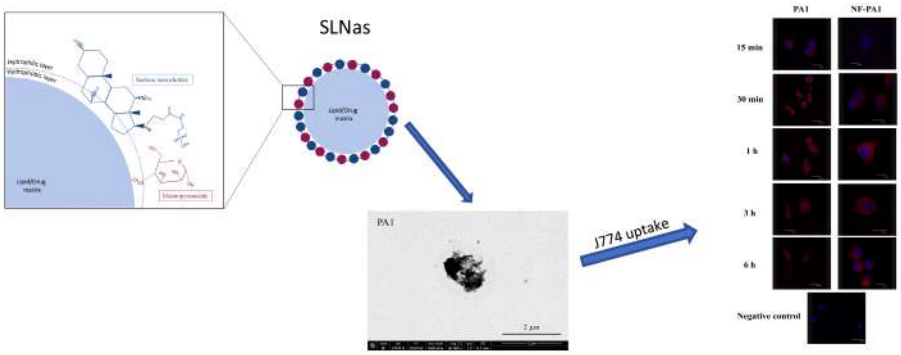

ACCEPTED MANUSCRIPT

Highlights

- Mannosylated SLN assemblies (SLNas) were investigated for inhaled anti-TB therapy
- Mannose residues were detected on SLNas surface
- Mannosylation proved to increase macrophage phagocytosis rate
- Mannosylation impaired SLNas respirability

Abstract

This study describes the development of new mannosylated Solid Lipid Nanoparticle assemblies (SLNas) delivering rifampicin for an inhaled treatment of tuberculosis. SLNas were surface engineered with mannose residues to recognize mannose receptors located on infected alveolar macrophages and facilitate cell internalization. Two sets of SLNas were produced by the melt emulsifying technique using biocompatible lipid components, i.e. cholesteryl myristate combined with palmitic acid (PA set) or tripalmitin (TP set), in the presence of the targeting moiety, methyl α-D-mannopyranoside. Mannosylated SLNas were examined for their physical properties, drug payloads and release, as well as respirability in terms of emitted dose and respirable fraction determined by Next Generation Impactor. The most appropriate formulations were assessed for mannosylation using FTIR, XPS, SEM coupled with EDX analysis, and wettability assay, in comparison with the respective non-functionalized SLNas. Besides, cytotoxicity and cell internalization ability were established on J774 murine macrophage cell line. Mannosylated SLNas exhibited physical properties suitable for alveolar macrophage passive targeting, adequate rifampicin payloads (10-15%), and feasible drug maintenance within SLNas along the respiratory tract before macrophage internalization. Despite respirability impaired by powder cohesiveness, surface mannosylation provided quicker macrophage phagocytosis, giving evidence of an active targeting promotion.

Keywords: Tuberculosis, Solid Lipid Nanoparticle assemblies, Inhalation, Surface mannosylation, Macrophage uptake

Chemical compounds studied in this article:

Palmitic acid (PubChem CID: 985)

Tripalmitin (PubChem CID: 11147)

Cholesteryl myristate (PubChem CID: 313252)

ACCEPTED MANUSCRIPT

Methyl α-D-mannopyranoside (PubChem CID: 101798)
Sodium taurocholate (PubChem CID: 23666345)
Rifampicin (PubChem CID: 5381226)

1. Introduction

Tuberculosis (TB) is caused by *Mycobacterium tuberculosis* (*Mtb*), which may attack any part of the body, but mainly the lungs. After being inhaled, *Mtb* reaches the alveoli where it is phagocytozed by alveolar macrophages (AM). Differently from any other microorganism, *Mtb* survives and causes the primary infection (González-Juarrero and O'Sullivan, 2011; WHO, 2016). The pulmonary route appears to be the most promising way to promptly reach the infected site in comparison with conventional administration routes (oral or intramuscular), leading to several advantages such as enhancement of local bioavailability by directly delivering the drug into the lungs, reduction in dose level and regimen dosage schedule, limitation of adverse drug reactions, and increase of patient compliance (Pham et al., 2015). The targeting of drugs to AM for diseases, such as TB, remains still an open question despite the rapid development in medicinal and drug delivery technologies. Two basic requirements need to be fulfilled in the design of inhaled formulations to achieve effective drug delivery inside AM. Firstly, drugs should be able to reach the target site after administration with minimal loss of their payload in the upper respiratory tract. Secondly, drugs should be taken up by AM. For water-insoluble drugs that must be administered by Dry Powder Inhaler (DPI) devices, passive targeting to alveoli in the deepest tract of the respiratory tract entails the development of particles with several essential properties namely narrow aerodynamic diameter range (0.5 – 5 μm), negative charge, non-spherical morphology, low density as well as high physical and chemical stability (Edwards, 2002; Iannuccelli and Maretti, 2015; Sihorkar and Vyas, 2001). However, it is extremely difficult that a particulate formulation can possess all these properties at the same time. In this regard, it is rare that unmodified drugs have features suitable for both DPI performance and AM targeting, thus failing to reach alveolar epithelium and penetrate AM effectively. Particle engineering techniques proposed different solutions for drug alone, drug/excipient blends (with lactose or mannitol) or carrier-based colloidal formulations (liposomes, polymeric/lipid micro- or nanoparticles, cyclodextrins) (Coowanitwong et al., 2008; Hirota et al., 2007; Kaur and Singh, 2014; Mohan et al., 2013; Son et al., 2011; Takenaga et al., 2008). Micro- and nanoparticles have been demonstrated to deliver high payload of drugs which are efficiently phagocytozed by AM in comparison to conventional dosage forms (Chono et al., 2007; Phanse et al., 2013; Singodia et al., 2012; Tiwari et al., 2011). A major advantage of using

ACCEPTED MANUSCRIPT

these formulations is the possibility of inserting molecules that recognize receptors on the target site at the particle surface. Among the various receptors, mannose receptors (MR), located on macrophages and overexpressed in infected AM, can recognize carriers bearing surface-exposed mannose residues and facilitate their internalization (Azad et al., 2014). A restricted number of researchers explored the targeting to MR using different drug delivery carriers to promote macrophage uptake in the treatment of TB. Solid Lipid Nanoparticles or Nanostructured Lipid Carriers modified by stearylamine for attaching mannose on the surface revealed a selective uptake from lung tissues compared to non-functionalized particles (Nimje et al., 2009; Pinheiro et al., 2016). Mannosylated gelatin nanoparticles encapsulating isoniazid exhibited safer and more efficient management of TB compared to plain nanoparticles and free drug (Saraogi et al., 2011). Polymeric micelles loaded with rifampicin, surface-decorated with chitosan and hydrolyzed galactomannan, were assayed on murine macrophages indicating that the carrier could not be efficiently taken up without the modification of the surface by galactomannan (Moretton et al., 2013).

Lipid micro-carriers arising from the assembly of Solid Lipid Nanoparticles (SLNas) for an inhaled anti-TB therapy by DPI devices were developed as a carrier of rifampicin (RIF), a first-line anti-TB drug, in our previous work. The designed SLNas were found to be respirable and effective for AM passive targeting (Maretti et al., 2016, 2014). The purpose of this work was to explore the possibility to maximize the phagocytosis process using mannosylated SLNas obtained by means of a novel functionalization technique avoiding chemical reactions thereby exhibiting manageability for scale-up production. The hypothesis that functionalization of particle surface influences the macrophage uptake was tested using a complementary suite of techniques. Lipid components were processed in the presence of sodium taurocholate as the biocompatible stabilizer and methyl α-D-mannopyranoside as the functionalizing agent. Two SLNas sets involving different lipid phases, drug/lipid ratios, and drug solubilization method within the lipid matrix were developed. The obtained mannosylated SLNas were examined for physico-chemical properties such as morphology, particle size, surface charge, *in vitro* aerodynamic performance, physical state of the components, drug loading and release. The optimized samples were investigated for the presence of mannose residues on the particle surface, cytotoxicity, and ability to be taken up by J774 macrophage cell line.

2. Materials and methods

2.1 Materials

ACCEPTED MANUSCRIPT

For SLNas preparation, tripalmitin and palmitic acid were purchased from Fluka Chemie (Buchs, Switzerland), sodium taurocholate (ST), methyl α-D-mannopyranoside (MP) and cholesteryl myristate from TCI Europe (Zwijndrecht, Belgium), and Nile Red from Sigma-Aldrich Italia (Milan, Italy). Rifampicin (RIF) was a gift from Sanofi (Brindisi, Italy). For SLNas characterization, Simulated Lung Fluid (SLF) at pH 7.4 was used according to Marques et al (Marques et al., 2011). The internal standard (IS) methyl parahydroxybenzoate was purchased from Carlo Erba Reagenti (Milan, Italy). For the cytotoxicity and cell internalization investigations, J774A.1 murine macrophage cell line from IZSLER (Brescia, Italy), cell culture reagents Dulbecco's Modification of Eagle's Medium (DMEM) with high glucose, L-glutamine, Fetal Bovine Serum (FBS), penicillin–streptomycin (P/S), non-essential amino acids (NEAA), and phosphate buffered saline (PBS) from EuroClone (Milan, Italy), Hoechst 33342 stain from ThermoFisher (Monza, Italy), and dimethyl sulfoxide (DMSO) from VWR (Milan, Italy) were purchased.

2.2 SLNas preparation

SLNas were prepared by emulsifying the melted lipids through sonication. Two sample sets were obtained by using cholesteryl myristate mixed with palmitic acid (PA set) or tripalmitin (TP set) as the lipid phase (Table 1). In practice, RIF was added to the lipid phase at 0.3:1 RIF/lipid ratio (PA1 and TP1 samples), melted at 85°C and emulsified in 20 mL Milli-Q water (highly pure water with a measured resistance of 18.2 MΩ cm^{-1} at 25°C, Millipore, USA) containing 2.25% (w/v) blend ST/MP at 1:2 ratio for the functionalized SLNas (SLNas) or 2.25% ST for the non-functionalized SLNas (NF-SLNas) as the aqueous phase by ultrasounds (14 output watts; Vibra-Cell, Sonics & Materials, Newtown, CT, USA) for 2 min, to obtain an oil-in-water (O/W) emulsion. To improve drug loading level, 0.5:1 RIF/lipid mass ratio (PA2 and TP2 samples) and the addition of 4 mL ethanol as co-solvent (PA2E and TP2E samples) were used. For cell internalization studies, labeled SLNas and NF-SLNas (PA1, TP2E, NF-PA1, and NF-TP2E samples) were obtained by dissolving Nile Red (0.01%) in the melted palmitic acid or tripalmitin. The emulsions were rapidly cooled in an ice bath under magnetic stirring for 15 min and the obtained particle suspension, in aliquots of 5 mL, was purified in 300 mL pH 7.4 PBS by dialysis membrane (MWCO 12–14000 Da, Medicell International Ltd., London, UK) for 15 min to remove the non-encapsulated drug and the excess of blend. Then, the samples were water diluted at 1:55 ratio, rapidly frozen at -70°C in a dry

ACCEPTED MANUSCRIPT

ice/acetone cooling bath and freeze-dried (Lyovac GT2, Leybold-Heraeus GmbH, Koln, Germany) to obtain a final powder according to the procedure previously optimized (Maretti et al., 2016).

2.3 Morphology, particle size, and Z-potential

SLNas morphology was evaluated by means of Scanning Electron Microscopy (SEM, Nova NanoSEM 450, Fei, Eindhoven, The Netherlands) using Transmission Electron Microscopy (TEM) mode with Scanning Transmission Electron Microscope (STEM) detector (30 kV). Carbon/copper TEM grids were soaked in a diluted particle water suspension and, after drying, coated with carbon under vacuum conditions (Carbon Coater, Balzers CED-010, Oerlikon Balzers, Balzers, Liechtenstein). Particle shape was investigated in terms of circularity parameter (value 1.0 indicates a perfect circle and value approaching zero indicates an increasingly irregular shape) measured on at least 250 particles by means of image processing software (ImageJ, CIGS, Modena, Italy) applied to TEM photomicrographs. Size and polydispersity index (PDI) were determined on SLNas before and after freeze-drying. In this latter case, SLNas were suspended in water for Zeta potential (Z-potential) and in DMEM containing FBS for size and PDI analyses. Size, expressed as median diameter of the main class (>85%), polydispersity index (PDI) and Z-potential were measured at a concentration of 0.1 g/L by using Photon Correlation Spectroscopy (PCS) (Zetasizer version 6.12, Malvern Instruments, Worcestershire, UK) equipped with a 4 mW He Ne laser (633 nm) and a DTS software (Version 5.0). The reported values averaged determinations on three batches.

2.4 SLNas stability

Particle size and PDI of all the samples, maintained for 6 months in a test tube inside dark glass vacuum desiccator at room temperature (25°C), were analyzed by the same methods described in section 2.3.

2.5 Rifampicin solubility

RIF solubility in both palmitic acid and tripalmitin was determined by visual observation of solution transparency. In detail, increasing amounts of RIF were added to 1 g melted lipid in a water bath at the SLNas preparation temperature (85°C). The maximum RIF amount giving a clear solution to the naked eye was recorded in triplicate.

ACCEPTED MANUSCRIPT

2.6 Drug loading and encapsulation efficiency

Drug loading, i.e. the percentage amount of RIF in SLNas freeze-dried powder, was determined by HPLC. RIF calibration solutions in the range from 12.8 to 51.2 mg/mL were prepared by dilutions of a stock methanolic solution and added with IS solution at a concentration of 30.08 mg/mL. For the analyzed SLNas samples, a 10.0 mg aliquot was weighted in a 10.0 mL volumetric flask and added with IS solution and methanol, heated at 50°C for 30 min and finally diluted (1:5) with methanol. The obtained samples were analyzed on a JASCO high-performance liquid chromatograph (Jasco Corporation, Tokyo, Japan) equipped with two PU-2080 Plus pumps, an HG-980-30 solvent mixing module and a UV-2075 Plus UV–Vis detector. Manual injection was performed by a Rheodyne 7725i injection valve (IDEX Corporation, Rohnert Park, CA, USA); the mobile phase was degassed during use by a solvent degasser mod. Degasys DG-1210 (Uniflows Co., Ltd., Tokyo, Japan). Chromatographic analysis was performed on a Purospher RP-18e column (125x4.0 mm; 5.0 µm) (Merck Darmstadt, Germany) with a mobile phase of (A) aqueous acetate buffer (pH 5.0; I = 0.02 M) and (B) methanol using the following gradient program: 0.0–5 min, isocratic at 60% (B); 5–10 min, linear gradient from 60 to 80% (B); 10 to 18 min, isocratic at 80% (B); 18 to 20 min, linear gradient from 80 to 60% (B). A pre-equilibration period of 15 min was used between each run. The flow rate was 0.9 mL/min and the column temperature was 30°C. The injection volume was 6.0 µL and the column eluates were monitored at 254 nm. Data were evaluated by Hercule Lite Chromatography Interface and Borwin Software, respectively (Jasco Corporation, Tokyo, Japan). The calibrators were analyzed in triplicate. Finally, encapsulation efficiency (EE%) values, expressed as the percentage of drug entrapped in SLNas (actual drug loading) compared to the initial amount of drug used in SLNas preparation (theoretical loading), were calculated.

2.7 Physical state of the components

Thermograms of SLNas (PA and TP sets), individual SLNas components as well as the respective physical mixtures prepared at the same drug/lipid ratio of SLNas were recorded by Differential Scanning Calorimeter (DSC) (DSC-4, Perkin-Elmer, Norwalk, CT, USA) in order to investigate the effect of the preparation process on the physical state of the components. DSC instrument was previously calibrated with indium. A heating rate of 10°C/min was employed over a temperature range of 30-300°C with nitrogen purging (30 mL/min). The analyses were performed in triplicate.

ACCEPTED MANUSCRIPT

2.8 In vitro drug release

In vitro RIF dissolution and release from SLNas samples were examined in sink conditions on exactly weighed samples (~100 mg) by means of the dialysis membrane (MWCO 12–14000 Da) method, in 30 mL of SLF. The system was maintained under gentle magnetic stirring to simulate the lung environment. Sample solutions (1 mL) were withdrawn at fixed intervals for a time period of 3 h and the initial volume restored. RIF quantification was performed spectrophotometrically (Lambda 35; Perkin-Elmer, Norwalk, CT, USA) in triplicate at the wavelength of 475 nm.

2.9 Fourier Transform Infra-Red (FTIR) spectroscopy

FTIR spectra of SLNas, NF-SLNas, and their individual components were obtained in Attenuated Total Reflectance (ATR) using FTIR spectrophotometer (FTIR Vertex 70 Bruker, Optics, Ettlingen, Germany) equipped with a Golden Gate Single Reflection Diamond ATR accessory (Specac, Orpington, UK) in the range of 4000–600 cm^{-1}. Depth of light penetration was in the range 0.7-2 µm for sample of Refractive Index 1.5 at 1000 cm^{-1}.

2.10 Elemental composition by Energy Dispersive X-ray (EDX) analysis

Elemental composition was determined by EDX analysis with X-EDS Bruker QUANTAX-200 (Bruker Nano GmbH, Berlin, Germany) coupled with SEM, with the aim of determining ST sulfur atoms. Elements can be identified qualitatively and semi-quantitatively in function of the X-ray energy emitted by their electrons transferring from a higher energy shell to a lower energy one. X-ray emission from Kα levels of the atoms oxygen (Kα= 0.525), carbon (Kα= 0.277), and sulfur (Kα= 2.307) were recorded by the selected area method from samples mounted without a conductive coating on copper TEM grids with the following experimental settings: accelerating voltage 30 kV, spot 1.5, detection limit < 0.1%, spatial resolution 0.1 µm. EDX spectra representing the plots of X-ray counts *vs.* elements. Semi-quantitative results were obtained and expressed as relative weight percentage of the elements present in the specimen. The reported data were averaged on three determinations for each sample.

2.11 X-ray Photoelectron Spectroscopy (XPS)

ACCEPTED MANUSCRIPT

XPS is the most widely used technique for analyzing a material in the 5 nm-thick surface layer of the sample. To determine the concentration of hydrophilic groups on the particle surface, XPS analysis was performed on the optimized SLNas and NF-SLNas samples by an analysis system 04–151 X-ray source (Physical Electronics, Chanhassen, MN, USA) and a hemispherical electron analyzer EA11 (Leybold Optics, Alzenau, Germany), using MgKα1,2 radiations (E=1253.6 eV). The spectra were recorded in fixed retardation ratio mode with 190 eV pass energy. The pressure in the sample analysis chamber was about 10^{-10} Torr. Data acquisition was performed with the RBD AugerScan 2. High-resolution data were collected using a pass energy of 50 eV in 0.1 eV steps-Spectra were analyzed for C1s peaks, in particular for C-O or C-OH bonds at 286.5 eV and for O1s peaks. In this latter case, it was possible to deconvolute the signals into two components, C=O at 531.8 eV and C-O or C-OH bonds at 533.1 eV. Curve fitting routines were performed with Igor Pro software. Signals were attributed on the basis of literature data (Bondioli et al., 2010).

2.12 Wettability

SLNas wettability was determined on 100 mg sample compressed in a hydraulic press (Perkin-Elmer, Norwalk, CT, USA) at 200 kg/cm^2 for 1 min using 12.5 mm diameter punches by direct measurement of the contact angle, the tangent angle at the contact point between a deionized water drop and the tablets at room temperature. The determinations were carried out in triplicate from three different batches.

2.13 Cell culture

J774 murine macrophage cell line, established from a reticulum cell sarcoma that arose in a female BALB/c mouse, was cultured as a monolayer in DMEM containing 2 mM L-glutamine, penicillin 100 UI/mL, 100 µg/mL streptomycin, NEAA 1X, and 10% FBS at 37°C in a humidified 5% CO_2 atmosphere. Cells were sub-cultured when the confluence was ≥ 80%. J774 cell line was selected as the most commonly used model to study the interaction with lung cells (Fytianos et al., 2016).

2.14 Cytotoxicity

J774 murine macrophage cell line was seeded at a density of 100,000 cells/well in 24-well tissue culture plates in complete DMEM. Cells were then incubated with 1 mL of SLNas suspension in complete medium at 0.25, 0.5, and 1.0 mg/mL particle dose (corresponding to 25, 50, and 100 µg

ACCEPTED MANUSCRIPT

RIF for PA set and 36.3, 72.5, and 145 µg RIF for TP set) for 15, 30 min, and 1, 3, 6 h incubation time. Furthermore, cells were incubated with 10 µl RIF ~~dissolved~~ solution in DMSO at ~~a~~ drug concentration range of 10-200 µg/mL for 24 h as the most common incubation period used for screening of antibiotic toxicity on macrophages (Pick et al., 2004) (10 µl DMSO as the control). After incubation times, cell viability was estimated by colorimetric 3-(4,5 di-methylthiazol-2-yl)-2,5-diphenyltetrazolium bromide (MTT) test according to the method described by Mosmann (Mosmann, 1983). MTT stock solution (5mg/mL in PBS) was added to each well at a volume of one-tenth the original culture and incubated for 2 h at 37°C in humidified CO_2. At the end of incubation periods, the medium was removed and the blue formazan crystals were solubilized by DMSO. MTT conversion to formazan by metabolically viable cells was monitored using a multiplate reader (TecanGenios Pro with Magellan 6 software, MTX Lab Systems, Bradenton, FL, USA) at an optical density of 535 nm. MTT test was performed in triplicate and cell viability was expressed as percentage of cell survival compared with untreated cells.

2.15 Cell internalization

SLNas and NF-SLNas were suspended in complete DMEM by vortex mixing for 1 min and sonic bath at 37°C for 3 min to a final particle amount of 0.25 mg/mL (equivalent to 26 µg/cm^2 cell monolayer). J774 cells were plated in 6-well plates (400,000 cells/well) and incubated with the sample suspension for 15, 30 min, and 1, 3, 6 h. After incubation, cells were washed three times with PBS to remove the possible SLNas adherent on cell membrane and then collected by gently scraper for flow cytometric analysis. Flow cytometry evaluation of intracellular uptake was performed by a Coulter Epics XL flow cytometer (Beckman Coulter Inc., Brea, CA, USA) equipped with an argon laser (488 nm). Analyses were done after recording at least 10,000 events for each sample. Results were expressed as percentages of fluorescence-positive cells.

J774 cells incubated with SLNas samples for 15, 30 min, and 1, 3, 6 h were fixed in paraformaldehyde (3%, w/v) for 30 min at room temperature, washed in PBS, and observed under filter set for red fluorescence (exciting wavelength of 525 nm, emission wavelength of 578 nm) by using confocal laser scanning microscopy (DMIRE2, Leica Microsystems GmbH, Wetzlar, Germany) at 1.1 µm step after cell nucleus staining by Hoechst 33342 stain (blue) (2 µg/mL) for 10 min at room temperature. The experiments were performed in triplicate.

2.16 Aerodynamic performance

ACCEPTED MANUSCRIPT

In vitro respirability of SLNas samples was determined using a Next Generation Impactor, NGI (Copley Scientific Ltd, Nottingham, UK) equipped with a micro-orifice collector (MOC) following the procedure detailed in the United States and European Pharmacopeias (European Pharmacopoeia, 2017b; The U.S Pharmacopeia, 2015b). The NGI was connected to a VP1000 S vacuum pump (Erweka GmbH, Heusenstamm, Germany). For each single experiment, a single dose ranging between 11 and 15 mg was discharged into the NGI. The powder was loaded into a size 3 capsule (V-Caps Capsugel, Morristown, New Jersey, USA) and aerosolized using a RS01 powder inhaler device (Plastiape spa, Lecco, Italy). A flow rate of 60 L/min, capable to produce a pressure drop of 4 kPa over the inhaler, was set before each experiment by a Flow Meter DFM 2000 (Copley Scientific, Nottingham, UK). RS01 was activated and the vacuum applied for 4 sec so that a volume of 4 L of air was drawn through the inhaler during the experiment. The measurement of the particles deposited in the impactor allowed the calculation of deposition parameters: Emitted Dose (ED) as the amount of SLNas measured from the induction port to the MOC; Respirable Fraction (RF) with size lower than 4.46 µm as the ratio between the cumulative mass of drug from S3 to MOC and ED. The experiments were performed in triplicate.

2.17 Angle of repose

The angle of repose is the constant, three-dimensional angle (relative to the horizontal base) assumed by a cone-like pile of material. Powders of PA1 and NF-PA1 are allowed to flow freely through a funnel, maintained 4 cm above the bench surface, onto the center of an upturned Petri dish of known radius according to United States and European Pharmacopeias (European Pharmacopoeia, 2017a; The U.S Pharmacopeia, 2015a). When the powder (500 mg) reaches the side of the Petri dish, the height of the cylindrical cone was determined. From the Petri dish radius (r, cm) and cone height (h, cm), the angle of repose α was calculated by the following equation:

$$\tan(\alpha) = \frac{h}{r}$$

Results were compared with the values reported on United States and European Pharmacopeias (European Pharmacopoeia, 2017a; The U.S Pharmacopeia, 2015a).

2.18 Statistical analysis

ACCEPTED MANUSCRIPT

Statistical analysis was performed by one-way Analysis of Variance (ANOVA). Significance was indicated by $p<0.05$ (*$p<0.05$; **$p<0.01$; ***$p<0.005$; ****$p<0.001$).

3. Results

3.1 SLNas formulations

Different lipid components, palmitic acid for PA set and tripalmitin for TP set, both in mixture with cholesteryl myristate and RIF under different conditions as described in ~~section 2.2~~ Table 1, were used to prepare Solid Lipid Nanoparticles assemblies (SLNas) by melt emulsification technique in the presence of sodium taurocholate (ST) as the surfactant. Methyl α-D-mannopyranoside (MP) was employed as the functionalizing agent to obtain mannosylated SLNas. Subsequently, SLNas were freeze-dried to obtain final dry powders.

3.2 SLNas characterization

3.2.1 Morphology, size, and surface charge

SLNas morphology and size were analyzed by TEM and PCS, respectively. Nanoparticles in water suspension before freeze-drying showed sizes from 0.39 ± 0.01 µm to 0.41 ± 0.03 µm with PDI value ranging from 0.23 ± 0.02 to 0.30 ± 0.02 without significant differences among all the samples ($p>0.05$). Freeze-dried SLNas, originating from aggregates of nanoparticles, exhibited irregular shape (Fig. 1) as confirmed by circularity values ranging from 0.45 ± 0.12 to 0.69 ± 0.01. The size range of SLNas main population was comprised from 0.72 ± 0.02 µm to 1.38 ± 0.19 µm and PDI values from 0.54 ± 0.09 to 0.81 ± 0.21. The use of ethanol as the co-solvent (PA2E and TP2E samples) provided slightly smaller SLNas (0.72 ± 0.02 µm and 0.80 ± 0.15 µm, respectively) without significant differences in PDI values (Table ~~1~~ 2). A minor population (<15%) showed size from 0.30 to 0.42 µm (online supplementary data, Fig. S1). Original SLNas dimensional properties (size and PDI) were found stable for at least six months without significant differences ($p<0.05$). SLNas Z-potential was highly negative (from -44.40 ± 4.59 mV to -63.7 ± 0.23 mV) (Table ~~1~~ 2) owing to the presence of anionic components. The most negative value was found in TP sample set. ~~SLNas samples were evaluated for RIF loading level by means of HPLC analysis. Drug loading and encapsulation efficiency (EE%) values ranged from 6.75 ± 0.03% to 14.53 ± 0.62% and from 25.53~~

ACCEPTED MANUSCRIPT

~~± 0.41% to 44.32 ± 1.59%, respectively (Table 1). PA1 and TP2E samples exhibited the highest values for each respective set.~~

3.2.2 DSC analysis

The physical state of SLNas was evaluated by means of DSC and compared with the corresponding drug/lipid physical mixtures and individual components. DSC thermograms of individual components are shown in Fig. 2a. SLNas thermal behavior revealed the endothermic peaks of palmitic acid (67.41°C), cholesteryl myristate (73.87°C), and tripalmitin (63.67°C). Unlike PA2, TP2, and physical mixtures exhibiting the thermal event of RIF (Fig. 2b,c), the peak was not detectable in PA1, TP1, PA2E, and TP2E samples.

3.2.3 Drug content and release

SLNas samples were evaluated for RIF loading level by means of HPLC analysis. Drug loading and encapsulation efficiency (EE%) values ranged from 6.75 ± 0.03% to 14.53 ± 0.62% and from 25.53 ± 0.41% to 44.32 ± 1.59%, respectively (Table ~~1~~ 2). ~~PA1 and TP2E samples exhibited the highest values for each respective set.~~

Drug release from PA and TP sets in comparison with RIF dissolution is shown in Fig. 3. Unlike drug dissolution that completed in about 1 h, RIF release was modulated by SLNas matrix. The release profile was monophasic, reaching about 30-50% of the payload in 3 h without notable differences among the samples.

Samples PA1 and TP2E that exhibited the highest levels of EE% and drug loading for each respective set~~, respectively,~~ were chosen to be further investigated. The presence of MP in PA1 and TP2E was evaluated in comparison with the respective samples obtained without MP, coded as non-functionalized PA1 (NF-PA1) and non-functionalized TP2E (NF-TP2E). All the properties measured for NF-PA1 and NF-TP2E samples did not exhibit ~~significant~~ remarkable differences in comparison with the respective functionalized samples (Table 2).

3.2.4 FTIR analysis

Unlike TP2E, MP characteristic bands at 3447 cm^{-1} and 3282 cm^{-1} associated with the hydroxyl groups (online supplementary data, Fig. S2) were not present in IR spectrum of PA1, probably owing to overlapped bands arising from palmitic acid hydroxyl group (online supplementary data,

ACCEPTED MANUSCRIPT

Fig. S3). The stretching bands of hydroxyl groups between 3600 and 3200 cm^{-1} were not observable in both NF-SLNas samples.

3.3 Surface mannosylation assessment

Energy Dispersive X-ray (EDX), X-ray Photoelectron Spectroscopy (XPS), and surface wettability analyses were used to assess the actual presence of mannose residues on SLNas surface. SLNas elemental composition was detected by means of EDX. The semi-quantitative results obtained for sulfur atoms, belonging to ST molecule, were expressed as relative weight percentage of the elements present in the specimen (Table ~~2~~ 3). PA1 and TP2E samples showed negligible characteristic sulfur X-ray emissions corresponding to sulfur abundances of 4.75 ± 1.21% and 9.14 ± 2.67%, respectively. On the contrary, NF-PA1 and NF-TP2E exhibited significantly ($p<0.05$) more relevant X-ray emissions from sulfur atoms corresponding to abundances of 15.71 ± 4.49% and 15.93 ±□4.01%, respectively.

XPS analysis of SLNas surface showed very little differences in C1s signal among the samples. ~~and O1s signals deconvoluted~~ On the contrary, deconvolution of O1s peaks into two components (C=O at 531.8 eV and C-O ~~together with~~ or C-OH at 533.1 eV, the latter two being present on the mannose moiety) ~~with~~ showed a different relative peak area. PA1 and TP2E samples, prepared in the presence of MP, exhibited a greater component concerning C-OH binding (36% and 43%, respectively) compared to NF-PA1 and NF-TP2E (28% and 36%, respectively) (Table ~~2~~ 3). Based on the consideration that the surface OH-group density is a major factor governing the wettability of materials, the contact angles of SLNas and NF-SLNas samples were measured (Table ~~2~~ 3). PA1 and TP2E samples provided smaller contact angles (31.18 ± 0.82° and 47.38 ± 6.91°, respectively), i.e. greater wettability than those of the equivalent NF-SLNas samples (34.90 ± 1.21° and 57.64 ± 2.25°, respectively).

3.4 In vitro cell culture assay

MTT test results obtained for PA1, TP2E, NF-PA1, and NF-TP2E samples, expressed as cell viability in function of the treatment time and dose, are shown in Fig. 4a-d. The reported data referred to cells incubated with particle amounts containing non-cytotoxic RIF doses. Concerning cells incubated with RIF in DMSO, a dose-dependent cytotoxicity at 24 h with a reduction of cell viability (<80%) was found starting from 100 µg/mL (Fig. 4e). TP2E and NF-TP2E resulted to be significantly ($p<0.05$) more cytotoxic than PA1 and NF-PA1 samples for all the incubation times

ACCEPTED MANUSCRIPT

and doses. On the contrary, there are no significant difference between PA1 and NF-PA1 samples (p>0.05). Therefore, PA1 and NF-PA1 samples at the dose of 0.25 mg/mL were selected for cell internalization assay. Flow cytometry data are shown in Fig. 5a. PA1 sample was taken up quickly by macrophages, reaching the intracellular fluorescence plateau (~25%) after 15 min without significant difference until the end of the experiment (p>0.05). On the contrary, the uptake of NF-PA1 sample exhibited a gradual fluorescence increase from ~10% to ~25%. In order to clarify ~~the~~ particle location inside the cells, confocal microscopy analysis was performed on J774 cell monolayer with blue stained nuclei. The images obtained under filter set for red and blue fluorescence from the cells incubated at different times with Nile Red labeled PA1 and NF-PA1 are shown in Fig. 5b. Cells incubated with PA1 sample revealed the presence of marked red fluorescent spots around the respective nuclei already at 15 min. Conversely, a negligible fluorescence was recorded from the cells incubated with NF-PA1 at both 15 and 30 min. Fluorescence comparable with that of PA1 sample appeared at 1 h and was maintained until the end of the experiment.

3.5 In vitro respirability and flowability

PA1, TP2E, NF-PA1, and NF-TP2E samples were assayed for respirability by NGI and flowability by angle of repose measurement. The ED value resulted ≥89% for all the samples. Both SLNas and NF-SLNas showed ~~a~~ favorable emission properties from the RS01 device. The calculation of Mass Median Aerodynamic Diameter (diameter at which 50% of the particles by mass are larger and 50% are smaller) was not possible since the particle mass deposited beyond Stage 1 was lower than 50% of the label dose as shown by the sample distribution in the impactor (online supplementary data, Fig. S4). The amount of RF with a respirable size (<4.46 µm) was calculated and was significantly (p<0.005) lower when SLNas were functionalized with MP. In detail, RF ranges of 2.04-2.85% and 17.85-25.23% were found for functionalized and non-functionalized SLNas, respectively, without significant differences between the sets (Table ~~2~~ 3). Regarding flowability, angle of repose in the range of 25-35° was found for PA1 and TP2E (34.23 ± 1.78° and 29.18 ± 2.20°, respectively) suggesting excellent/good sliding powders. Significant higher angles (p<0.05) in the range of 41-55° were found for NF-PA1 (45.68 ± 5.23°) and NF-TP2E (45.46 ± 0.65°) indicating passable/poor flow ability (Table ~~2~~ 3).

4. Discussion

ACCEPTED MANUSCRIPT

The effective treatment of TB disease could be successfully addressed with the development of carriers able to deliver existing drugs in a more efficient way to the target tissue. This study explores the specific targeting of a clinically used anti-TB drug by means of surface engineering of Solid Lipid Nanoparticle assemblies (SLNas) delivered to alveolar macrophages (AM), the site of primary infection, by pulmonary route. The success of lipid carriers, known to be biocompatible and biodegradable, is based on a careful selection of materials as well as an evaluation of the particle physical characteristics and surface features. Other Authors dealt with surface modification of drug carriers, but these efforts were based on complex chemical reactions critical for a scale-up perspective (Moretton et al., 2013; Nimje et al., 2009; Pinheiro et al., 2016; Saraogi et al., 2011). Moreover, to our knowledge, the effect of surface mannosylation of inhaled particulate carriers on respirability was not reported in literature. The present research was directed to a new surface functionalization approach by mixing mannopyranoside (MP) as the functionalizing agent with sodium taurocholate (ST) as the surfactant avoiding synthetic processes. A mixture of cholesteryl myristate with palmitic acid or tripalmitin was selected as the lipid matrix for SLNas owing to their melt-processable characteristics and low cytotoxicity (Dal Pizzol et al., 2014; Martins de Lima et al., 2006). A blend of ST/MP at 1:2 ratio proved to be the most efficient in preliminary studies. Moreover, formulation components were processed by means of a methodology already optimized to obtain respirable powders (Maretti et al., 2016). The effect of both lipid phase composition and surface SLNas mannosylation on respirability performance and promotion of macrophage active targeting was assessed.

Regarding pulmonary treatment of intramacrophagic bacteria, microparticles are considered more active than nanoparticles, especially in terms of respirability associated with the emission by DPI device and deposition onto alveolar epithelium. For this reason, hybrid vectors in which nanoparticles are embedded in microparticulate shells were developed by a few Authors (Fattal et al., 2014; Tee et al., 2015). This technological approach allows to improve the aerodynamic properties of native nanoparticles with a size smaller than 0.5 μm that are mostly exhaled without deposition onto alveolar region (Iannuccelli and Maretti, 2015). At the same time, particles larger than 2 or 5 μm have a lower possibility of bypassing the upper airways (Lee et al., 2015; Scalia et al., 2015; Taylor, 2007). SLNas appear to be in agreement with these requirements being irregular microsized nanoparticle aggregates that formed during freeze-drying process by the adhesion of the un-dried nanosized particles. The fraction of non-aggregated nanoparticles generated a minor dimensional population having the same size of the un-dried nanoparticles, accounting for the higher PDI values of freeze-dried samples in comparison to the un-dried ones. Beyond the size, the irregular shape exhibited by SLNas plays a relevant role in powder aerodynamic performance

ACCEPTED MANUSCRIPT

providing better powder de-aggregation and fluidization capacity due to the lower particle contact area (Claus et al., 2014; Son et al., 2011). Moreover, SLNas negative surface charge, due to the contribution from all the particle components, is a favorable property giving lower cytotoxicity compared to positive or neutral particles and promoting the internalization process by AM (Bhattacharjee et al., 2010; Brandhonneur et al., 2009; Kelly et al., 2010; Vyas et al., 2004). However, besides the suitable physical properties, inhaled particulate carriers require sufficient drug payload to achieve a therapeutic effect in function of a feasible administration dose inside DPI device and negligible drug spreading over the lung fluid before AM uptake. Lipids are the most appropriate carrier materials to embed lipophilic drugs such as RIF. The highest EE% values within each set were obtained by using both 0.3:1 RIF/palmitic acid ratio (PA1) providing about 10% drug loading and 0.5:1 RIF/tripalmitin ratio using the co-solvent (TP2E) providing about 14% drug loading, without significant difference between the two EE% values. This finding could be related to RIF solubility, higher in palmitic acid (around 6%, w/w) compared to tripalmitin (around 1%, w/w). The obtained RIF payloads are in the common range of values associated with particulate systems for TB inhalation therapy (Muttil et al., 2007). By considering that efficient RIF inhaled doses were found lower than the oral ones both in humans and in animal models (Garcia Contreras et al., 2015; Katiyar et al., 2008; Parikh et al., 2013), a feasible SLNas dose could be reasonably introduced in a DPI device (Zhu et al., 2015). Indeed, it was demonstrated that the mean concentration of inhaled rifampicin inside alveolar macrophages was 113 times higher than that achieved following oral administration (Katiyar et al., 2008). Therefore, the common daily dosage of maximum 600 mg orally administered could be replaced by inhaled doses of about 6.0 mg RIF higher than MIC (0.5 µg/mL) (Ziglam et al., 2002) corresponding to about 60 mg PA1 sample and 43 mg TP2E sample. Such SLNas amounts could be formulated in commercial DPI devices.

Thermal analysis indicated that RIF raw material was in its polymorphic form II as indicated by the endothermic event at 188°C corresponding to the melting process followed by recrystallization in polymorph I (exothermic event at 190°C) with decomposition at 242°C. Regarding the effect of the drug/lipid ratio and the co-solvent on RIF physical state, PA2 and TP2 samples showed a similar RIF physical state to that observed in the raw material, whereas an amorphous state of the drug was exhibited at the lower drug/lipid ratio (PA1 and TP1 samples) and at the highest drug/lipid ratio only in the presence of the co-solvent (PA2E and TP2E samples) (Alves et al., 2010; Panchagnula and Bhardwaj, 2008). The different RIF physical states and loading levels did not influence drug release from SLNas. Unlike drug dissolution reaching about 90% in 1 h, RIF was delivered gradually from SLNas, regardless of the sample, reaching release percentages ranging from about 30 to 50% of the payload in 3 h. Because of 10-20% RIF release in about 30 min and quick

ACCEPTED MANUSCRIPT

macrophage endocytic process (Alexis et al., 2006; Geiser, 2002; Muttil et al., 2007; Parikh et al., 2013; Wang et al., 2014), the carrier would be able to avoid drug spreading over the lung fluid before AM uptake allowing the consequent intracellular drug delivery.

Although all the samples were found to be appropriate concerning their physical characteristics, only PA1 and TP2E that exhibited the highest EE% and drug loading levels were investigated for mannose surface functionalization in comparison with NF-SLNas samples. The expected arrangement of ST/MP blend on the lipid matrix surface is schematically shown in Fig. 6. MP would orientate with the non-polar tail (methyl group) towards SLNas lipid matrix leaving the polar head including OH-groups free. ST is an anionic surfactant composed by cholic acid consisting of carbocyclic rings and taurine carrying a sulfonic acid group that imparts the negative charge onto the molecule at physiological pH. This molecule shows an unusual behavior, which is related to its molecular architecture. The hydrophilic and hydrophobic parts of the molecule are located on the opposite faces of the steroid nucleus. The face containing hydroxyl groups and taurine indicates the hydrophilic side, while the face containing methyl groups indicates the hydrophobic side that ties the lipid matrix (Verde and Frenkel, 2010). Therefore, the hydrophilic external layer of SLNas would be composed by taurine present in ST molecule and -OH groups belonging to both ST and MP. The more abundant density of MP -OH groups determined the higher wettability and the greater XPS output of SLNas in comparison with NF-SLNas samples. On the other hand, the lower amount of taurine sulfur atoms in SLNas in comparison with NF-SLNas, as indicated by EDX analysis, confirms the partial replacement of ST molecules by MP on the particle surface. Therefore, all the results of the analyses performed contribute to support the hypothesis that the mannose derivative remained lipid associated despite the procedure steps under water environment, reasonably owing to hydrophobic interactions occurring between MP methyl group and the matrix lipids.

The evaluation of the actual active targeting to AM as a result of SLNas surface functionalization was performed only on the non-cytotoxic PA1 and NF-PA1 samples. Since all the SLNas components are known as Generally Recognized As Safe (GRAS) and component of tracheobronchial secretions or additives in marketed pulmonary surfactants (Nakahara et al., 2011; Pilcer and Amighi, 2010; Slomiany et al., 1982; Zuo et al., 2008), TP2E and NF-TP2E cytotoxicity could be attributed to more aggregates that lead to decrease in cell activity and even to death (He et al., 2011). The faster uptake of PA1 sample by macrophage cell line compared with that of NF-PA1, as highlighted by flow cytometry and confocal microscopy, is ascribable to the presence of mannose residues on the particle surface, since all the other properties were equivalent. Although the successful results in the internalization process of mannosylated particles, surface modifications

ACCEPTED MANUSCRIPT

could influence negatively the aerodynamic performance and compromise powder de-aggregation from the device and ability to deposit in the respiratory/alveolar region. Concerning flowability, mannosylation provided an improvement of flow properties, as demonstrated by angle of repose values, that could promote an efficient emptying of the particles upon actuation of the inhaler device and hence a reproducible emitted dose. Accordingly, emitted dose values were not invalidated by the surface modification and complied with the pharmacopeial requirements establishing that more than 75% of the loaded dose should leave the device upon inhalation (European Pharmacopoeia, 2017b; The U.S Pharmacopeia, 2015b). Nevertheless, mannosylation determined a massive reduction in respirability probably because of both moisture adsorption on mannose residues and high adhesion forces among mannose hydroxyl groups that could make the powder cohesive (Bosquillon et al., 2004, 2001; Martinelli et al., 2017; Yang et al., 2005).

5. Conclusions

The efficient inhalation of anti-TB drugs loaded into particulate carriers is governed by multiple interrelated parameters leading to particle deposition over the alveolar epithelium and phagocytosis by alveolar macrophages (AM). In the present study, aggregates of SLN (SLNas), adequate for the purpose of an AM passive targeting, were successfully surface engineered by methyl α-D-mannopyranoside (MP) for an active targeting using a simple technology, feasible in a scale-up perspective. Despite favorable physical properties including size, morphology, surface charge, and emitted doses by DPI device, respirability was impaired by the particle cohesiveness especially when SLNas were functionalized. Concerning the active targeting, MP presence on SLNas surface caused an improvement of the internalization rate by macrophages with a potential increase in drug release inside the cells. Owing to the effectiveness of mannose in AM uptake process, more balanced amphiphiles bearing α-D-mannose residues capable to protect powder from environmental moisture reducing powder cohesion and improving particle de-aggregation and respirability will be evaluated in the future step of investigation.

Declaration of interest

No conflicts of interest exist.

Acknowledgment

ACCEPTED MANUSCRIPT

The authors thank Fondazione di Vignola for the financial support. Thanks to Prof. Gilberto Coppi, Dr. Mauro Zapparoli, and Dr. Cinzia Restani for their excellent assistance.

References

Alexis, N.E., Lay, J.C., Zeman, K.L., Geiser, M., Kapp, N., Bennett, W.D., 2006. In Vivo Particle Uptake by Airway Macrophages in Healthy Volunteers. Am. J. Respir. Cell Mol. Biol. 34, 305–313.

Alves, R., Reis, T.V. da S., Silva, L.C.C. da, Storpírtis, S., Mercuri, L.P., Matos, J. do R., 2010. Thermal behavior and decomposition kinetics of rifampicin polymorphs under isothermal and non-isothermal conditions. Braz. J. Pharm. Sci. 46, 343–351.

Azad, A.K., Rajaram, M.V.S., Schlesinger, L.S., 2014. Exploitation of the Macrophage Mannose Receptor (CD206) in Infectious Disease Diagnostics and Therapeutics. J. Cytol. Mol. Biol. 1, 1000003.

Bhattacharjee, S., de Haan, L.H.J., Evers, N.M., Jiang, X., Marcelis, A.T.M., Zuilhof, H., Rietjens, I.M.C.M., Alink, G.M., 2010. Role of surface charge and oxidative stress in cytotoxicity of organic monolayer-coated silicon nanoparticles towards macrophage NR8383 cells. Part. Fibre Toxicol. 7, 25.

Bondioli, L., Costantino, L., Ballestrazzi, A., Lucchesi, D., Boraschi, D., Pellati, F., Benvenuti, S., Tosi, G., Vandelli, M.A., 2010. PLGA nanoparticles surface decorated with the sialic acid, N-acetylneuraminic acid. Biomaterials 31, 3395–3403.

Bosquillon, C., Lombry, C., Préat, V., Vanbever, R., 2001. Influence of formulation excipients and physical characteristics of inhalation dry powders on their aerosolization performance. J. Control. Release 70, 329–339.

Bosquillon, C., Rouxhet, P.G., Ahimou, F., Simon, D., Culot, C., Préat, V., Vanbever, R., 2004. Aerosolization properties, surface composition and physical state of spray-dried protein powders. J. Control. Release 99, 357–367.

Brandhonneur, N., Chevanne, F., Vié, V., Frisch, B., Primault, R., Le Potier, M.-F., Le Corre, P., 2009. Specific and non-specific phagocytosis of ligand-grafted PLGA microspheres by macrophages. Eur. J. Pharm. Sci. 36, 474–485.

ACCEPTED MANUSCRIPT

Chono, S., Tanino, T., Seki, T., Morimoto, K., 2007. Uptake characteristics of liposomes by rat alveolar macrophages: influence of particle size and surface mannose modification. J. Pharm. Pharmacol. 59, 75–80.

Claus, S., Weiler, C., Schiewe, J., Friess, W., 2014. How can we bring high drug doses to the lung? Eur. J. Pharm. Biopharm. 86, 1–6.

Coowanitwong, I., Arya, V., Kulvanich, P., Hochhaus, G., 2008. Slow Release Formulations of Inhaled Rifampin. AAPS J. 10, 342–348.

Dal Pizzol, C., Filippin-Monteiro, F.B., Restrepo, J.A.S., Pittella, F., Silva, A.H., de Souza, P.A., de Campos, A.M., Creczynski-Pasa, T.B., 2014. Influence of Surfactant and Lipid Type on the Physicochemical Properties and Biocompatibility of Solid Lipid Nanoparticles. Int. J. Environ. Res. Public. Health 11, 8581–8596.

Edwards, D.A., 2002. Delivery of biological agents by aerosols. AIChE J. 48, 2–6.

European Pharmacopoeia 9th ed. 2017a. Powder flow, 2.09.36.

European Pharmacopoeia 9th ed. 2017b. Preparations for Inhalation, 2.09.18.

Fattal, E., Grabowski, N., Mura, S., Vergnaud, J., Tsapis, N., Hillaireau, H., 2014. Lung toxicity of biodegradable nanoparticles. J. Biomed. Nanotechnol. 10, 2852–2864.

Fytianos, K., Drasler, B., Blank, F., von Garnier, C., Seydoux, E., Rodriguez-Lorenzo, L., Petri-Fink, A., Rothen-Rutishauser, B., 2016. Current in vitro approaches to assess nanoparticle interactions with lung cells. Nanomed. 11, 2457–2469.

Garcia Contreras, L., Sung, J., Ibrahim, M., Elbert, K., Edwards, D., Hickey, A., 2015. Pharmacokinetics of Inhaled Rifampicin Porous Particles for Tuberculosis Treatment: Insight into Rifampicin Absorption from the Lungs of Guinea Pigs. Mol. Pharm. 12, 2642–2650.

Geiser, M., 2002. Morphological aspects of particle uptake by lung phagocytes. Microsc. Res. Tech. 57, 512–522.

González-Juarrero, M., O'Sullivan, M.P., 2011. Optimization of inhaled therapies for tuberculosis: The role of macrophages and dendritic cells. Tuberculosis 91, 86–92.

He, P., Tao, J., Xue, J., Chen, Y., 2011. Cytotoxicity Property of nano-TiO2 Sol and nano-TiO2 Powder. J. Nanomater. 2011, 20:20–20:20.

ACCEPTED MANUSCRIPT

Hirota, K., Hasegawa, T., Hinata, H., Ito, F., Inagawa, H., Kochi, C., Soma, G.-I., Makino, K., Terada, H., 2007. Optimum conditions for efficient phagocytosis of rifampicin-loaded PLGA microspheres by alveolar macrophages. J. Control. Release 119, 69–76.

Iannuccelli, V., Maretti, E., 2015. Inhaled Micro- or Nanoparticles: Which are the Best for Intramacrophagic Antiinfectious Therapies? J. Infect. Dis. Diagn. 1, e102.

Katiyar, S.K., Bihari, S., Prakash, S., 2008. Low-dose inhaled versus standard dose oral form of anti-tubercular drugs: concentrations in bronchial epithelial lining fluid, alveolar macrophage and serum. J. Postgrad. Med. 54, 245–246.

Kaur, I.P., Singh, H., 2014. Nanostructured drug delivery for better management of tuberculosis. J. Control. Release 184, 36–50.

Kelly, C., Jefferies, C., Cryan, S.-A., 2010. Targeted Liposomal Drug Delivery to Monocytes and Macrophages. J. Drug Deliv. 2011, e727241.

Lee, W.-H., Loo, C.-Y., Traini, D., Young, P.M., 2015. Nano- and micro-based inhaled drug delivery systems for targeting alveolar macrophages. Expert Opin. Drug Deliv. 12, 1009–1026.

Maretti, E., Rossi, T., Bondi, M., Croce, M.A., Hanuskova, M., Leo, E., Sacchetti, F., Iannuccelli, V., 2014. Inhaled Solid Lipid Microparticles to target alveolar macrophages for tuberculosis. Int. J. Pharm. 462, 74–82.

Maretti, E., Rustichelli, C., Romagnoli, M., Balducci, A.G., Buttini, F., Sacchetti, F., Leo, E., Iannuccelli, V., 2016. Solid Lipid Nanoparticle assemblies (SLNas) for an anti-TB inhalation treatment—A Design of Experiments approach to investigate the influence of pre-freezing conditions on the powder respirability. Int. J. Pharm. 511, 669–679.

Marques, M.R.C., Loebenberg, R., Almukainzi, M., 2011. Simulated Biological Fluids with Possible Application in Dissolution Testing. Dissolution Technol. 18, 15–28.

Martinelli, F., Balducci, A.G., Kumar A., Sonvico, F., Forbes, B., Bettini, R., Buttini, F., 2017. Engineered sodium hyaluronate respirable dry powders for pulmonary drug delivery. Int. J. Pharm. 517, 286–295.

Martins de Lima, T., Cury-Boaventura, M.F., Giannocco, G., Nunes, M.T., Curi, R., 2006. Comparative toxicity of fatty acids on a macrophage cell line (J774). Clin. Sci. Lond. Engl. 1979 111, 307–317.

ACCEPTED MANUSCRIPT

Mohan, A., Kumar, D.P., Harikrishna, J., 2013. Newer Anti-TB Drugs and Drug Delivery Systems, in: Medicine Update. The Association of Physicians of India, vol 23.

Moretton, M.A., Chiappetta, D.A., Andrade, F., das Neves, J., Ferreira, D., Sarmento, B., Sosnik, A., 2013. Hydrolyzed galactomannan-modified nanoparticles and flower-like polymeric micelles for the active targeting of rifampicin to macrophages. J. Biomed. Nanotechnol. 9, 1076–1087.

Mosmann, T., 1983. Rapid colorimetric assay for cellular growth and survival: Application to proliferation and cytotoxicity assays. J. Immunol. Methods 65, 55–63.

Muttil, P., Kaur, J., Kumar, K., Yadav, A.B., Sharma, R., Misra, A., 2007. Inhalable microparticles containing large payload of anti-tuberculosis drugs. Eur. J. Pharm. 32, 140–150.

Nakahara, H., Lee, S., Shoyama, Y., Shibata, O., 2011. The role of palmitic acid in pulmonary surfactant systems by Langmuir monolayer study: Lipid–peptide interactions. Soft Matter. 7, 11351-11359.

Nimje, N., Agarwal, A., Saraogi, G.K., Lariya, N., Rai, G., Agrawal, H., Agrawal, G.P., 2009. Mannosylated nanoparticulate carriers of rifabutin for alveolar targeting. J. Drug Target. 17, 777–787.

Panchagnula, R., Bhardwaj, V., 2008. Effect of amorphous content on dissolution characteristics of rifampicin. Drug Dev. Ind. Pharm. 34, 642–649.

Parikh, R., Patel, L., Dalwadi, S., 2013. Microparticles of rifampicin: comparison of pulmonary route with oral route for drug uptake by alveolar macrophages, phagocytosis activity and toxicity study in albino rats. Drug Deliv. 21, 406–411.

Pham, D.-D., Fattal, E., Tsapis, N., 2015. Pulmonary drug delivery systems for tuberculosis treatment. Int. J. Pharm. 478, 517–529.

Phanse, Y., Carrillo-Conde, B.R., Ramer-Tait, A.E., Roychoudhury, R., Pohl, N.L.B., Narasimhan, B., Wannemuehler, M.J., Bellaire, B.H., 2013. Functionalization of polyanhydride microparticles with di-mannose influences uptake by and intracellular fate within dendritic cells. Acta Biomater. 9, 8902–8909.

Pick, N., Cameron, S., Arad, D., Av-Gay, Y., 2004. Screening of Compounds Toxicity against Human Monocytic cell line-THP-1 by Flow Cytometry. Biol. Proced. Online. 6, 220-225.

ACCEPTED MANUSCRIPT

Pilcer, G. and Amighi, K., 2010. Formulation strategy and use of excipients in pulmonary drug delivery. Int. J. Pharm. 392, 1-19.

Pinheiro, M., Ribeiro, R., Vieira, A., Andrade, F., Reis, S., 2016. Design of a nanostructured lipid carrier intended to improve the treatment of tuberculosis. Drug Des. Devel. Ther. 10, 2467–2475.

Saraogi, G.K., Sharma, B., Joshi, B., Gupta, P., Gupta, U.D., Jain, N.K., Agrawal, G.P., 2011. Mannosylated gelatin nanoparticles bearing isoniazid for effective management of tuberculosis. J. Drug Target. 19, 219–227.

Scalia, S., Young, P.M., Traini, D., 2015. Solid lipid microparticles as an approach to drug delivery. Expert Opin. Drug Deliv. 12, 583–599.

Sihorkar, V., Vyas, S.P., 2001. Potential of polysaccharide anchored liposomes in drug delivery, targeting and immunization. J. Pharm. Pharm. 4, 138–158.

Singodia, D., Verma, A., Verma, R.K., Mishra, P.R., 2012. Investigations into an alternate approach to target mannose receptors on macrophages using 4-sulfated N-acetyl galactosamine more efficiently in comparison with mannose-decorated liposomes: an application in drug delivery. Nanomedicine Nanotechnol. Biol. Med. 8, 468–477.

Slomiany, A., Murty, V.L., Aono, M., Snyder, C.E., Herp, A., Slomiany, B.L., 1982. Lipid composition of tracheobronchial secretions from normal individuals and patients with cystic fibrosis. Biochim. Biophys. Acta. 710, 106-111.

Son, Y.-J., Mitchell, J.P., McConville, J.T., 2011. In Vitro Performance Testing for Pulmonary Drug Delivery, in: Smyth, H.D.C., Hickey, A.J. (Eds.), Controlled Pulmonary Drug Delivery. Springer New York, pp. 383–415.

Takenaga, M., Ohta, Y., Tokura, Y., Hamaguchi, A., Igarashi, R., Disratthakit, A., Doi, N., 2008. Lipid Microsphere Formulation Containing Rifampicin Targets Alveolar Macrophages. Drug Deliv. 15, 169–175.

Taylor, K.M.G., 2007. Pulmonary drug delivery, in: Aulton's Pharmaceutics: The Design and Manufacture of Medicines. 4th ed. Aulton M.E. and Taylor K.M.G. Eds; Churchill Livingstone Elsevier: Edinburgh, New York, pp 638-657.

ACCEPTED MANUSCRIPT

Tee, N., Zhu, Y., Mortimer, G.M., Martin, D.J., Minchin, R.F., 2015. Fluoromica nanoparticle cytotoxicity in macrophages decreases with size and extent of uptake. Int. J. Nanomedicine 10, 2363–2375.

The United States Pharmacopeia 37 and National Formulary 32, 2015a. Powder flow; 1174.

The United States Pharmacopeia 37 and National Formulary 32, 2015b. Aerosols, Nasal, Sprays, Metered-Dose Inhalers, and Dry Powder Inhalers; 601.

Tiwari, S., Chaturvedi, A.P., Tripathi, Y.B., Mishra, B., 2011. Macrophage-specific targeting of isoniazid through mannosylated gelatin microspheres. AAPS PharmSciTech 12, 900–908.

Verde, A.V., Frenkel, D., 2010. Simulation study of micelle formation by bile salts. Soft Matter 6, 3815–3825.

Vyas, S.P., Kannan, M.E., Jain, S., Mishra, V., Singh, P., 2004. Design of liposomal aerosols for improved delivery of rifampicin to alveolar macrophages. Int. J. Pharm. 269, 37–49.

Wang, Y.-B., Watts, A.B., Peters, J.I., Williams, R.O., 2014. The impact of pulmonary diseases on the fate of inhaled medicines--a review. Int. J. Pharm. 461, 112–128.

World Health Organization, Global Tuberculosis Report 2016. The Organization, Geneva, Switzerland.

Yang, J., Sliva, A., Banerjee, A., Dave, R.N., Pfeffer, R., 2005. Dry particle coating for improving the flowability of cohesive powders. Powder Technol. 158, 21–33.

Zhu, B., Young, P.M., Ong, H.X., Crapper, J., Flodin, C., Qiao, E.L., Phillips, G., Traini, D., 2015. Tuning aerosol performance using the multibreath Orbital® dry powder inhaler device: controlling delivery parameters and aerosol performance via modification of puck orifice geometry. J. Pharm. Sci. 104, 2169–2176.

Ziglam, H.M., Baldwin, D.R., Daniels, I., Andrew, J.M., Finch, R.G., 2002. Rifampicin concentrations in bronchial mucosa, epithelial lining fluid, alveolar macrophages and serum following a single 600mg oral dose in patients undergoing fibre-optic bronchoscopy. J. Antimicrob. Chemother. 50, 1011–1015.

Zuo, Y.Y., Veldhuizen, R.A.W., Neumann, A.W., Petersen, N.O., Possmayer, O., 2008. Current perspectives in pulmonary surfactant — Inhibition, enhancement and evaluation. Biochim. Biophys. Acta. 1778, 1947-1977.

ACCEPTED MANUSCRIPT

Table 1.
Lipid phase composition of PA and TP sample sets

PA set		TP set	
PA1	175 mg palmitic acid 75 mg cholesteryl myristate 75 mg RIF	**TP1**	175 mg tripalmitin 75 mg cholesteryl myristate 75 mg RIF
PA2	175 mg palmitic acid 75 mg cholesteryl myristate 125 mg RIF	**TP2**	175 mg tripalmitin 75 mg cholesteryl myristate 125 mg RIF
PA2E	175 mg palmitic acid 75 mg cholesteryl myristate 125 mg RIF 4 mL ethanol	**TP2E**	175 mg tripalmitin 75 mg cholesteryl myristate 125 mg RIF 4 mL ethanol

ACCEPTED MANUSCRIPT

Table ~~1~~ 2.
Physical characteristics, drug loading, and encapsulation efficiency (EE%) of SLNas samples (mean values ± SD)

Sample	Size (µm)	PDI	Circularity	Z-potential (mV)	Drug loading (%, w/w)	EE%
PA1	1.38 ± 0.19	0.54 ± 0.09	0.61 ± 0.05	-45.33 ± 0.81	10.23 ± 0.26	44.32 ± 1.59
PA2	1.19 ± 0.26	0.78 ± 0.21	0.62 ± 0.03	-55.50 ± 0.95	9.78 ± 0.48	29.34 ± 1.70
PA2E	0.72 ± 0.02	0.70 ± 0.22	0.54 ± 0.06	-44.40 ± 4.59	8.51 ± 0.14	25.53 ± 0.41
TP1	1.04 ± 0.03	0.78 ± 0.10	0.62 ± 0.05	-60.00 ± 0.53	6.75 ± 0.03	29.03 ± 0.06
TP2	0.99 ± 0.02	0.81 ± 0.21	0.45 ± 0.12	-57.87 ± 1.58	10.71 ± 0.24	32.13 ± 0.71
TP2E	0.80 ± 0.15	0.72 ± 0.12	0.69 ± 0.01	-63.70 ± 0.23	14.53 ± 0.62	43.60 ± 1.86
NF-PA1	1.17 ± 0.12	0.74 ± 0.07	0.65 ± 0.03	-55.5 ± 0.95	6.87 ± 0.36	29.72 ± 0.25
NF-TP2E	0.89 ± 0.11	0.47 ± 0.15	0.72 ± 0.07	-54.93 ± 1.21	12.99 ± 0.42	38.97 ± 0.06

ACCEPTED MANUSCRIPT

Table ~~2~~ 3.
Surface and inhalation properties of SLNas samples (mean values ± SD) evaluated by EDX (*), XPS (**), and NGI (***) analyses

Sample	S weight (%)*	C=O (%)**	C-O or C-OH (%)**	Contact angle (°)	ED (%)***	RF < 4.46 µm (%)***	Angle of repose (°)
PA1	4.75 ± 1.21	64	36	31.18 ± 0.82	97.07 ± 0.21	2.85 ± 1.38	34.23 ± 1.78
NF-PA1	15.71 ± 4.49	72	28	34.90 ± 1.21	89.19 ± 1.72	25.23 ± 0.74	45.68 ± 5.32
TP2E	9.14 ± 2.67	57	43	47.38 ± 6.91	97.65 ± 0.15	2.04 ± 0.14	29.18 ± 2.20
NF-TP2E	15.93 ± 4.01	64	36	57.64 ± 2.25	94.51 ± 1.38	17.85 ± 1.97	45.46 ± 0.65

~~*EDX analysis~~
~~** XPS analysis~~
~~***NGI analysis~~

ACCEPTED MANUSCRIPT

Figure Captions

Fig. 1. TEM images of SLNas samples

Fig. 2. DSC thermograms of (a) SLNas components, (b) PA, and (c) TP sample sets with the respective physical mixtures

Fig. 3. RIF dissolution and release from (a) PA and (b) TP sample sets

Fig. 4. SLNas cytotoxicity on J774 cell line: (a) PA1, (b) NF-PA1, (c) TP2E, and (d) NF-TP2E samples at different doses (0.25, 0.5, and 1 mg/mL) and growing incubation times (15, 30 min, and 1, 3, 6 h) (dotted line as the control); (e) RIF cytotoxicity at 24 h incubation time (DMSO as the control). Statistical significance levels are indicated as: * ($p<0.05$); ** ($p<0.01$); *** ($p<0.005$); **** ($p<0.001$)

Fig. 5. (a) Cytometric analysis of PA1 and NF-PA1 samples at 0.25 mg/mL dose on J774 cell line at growing incubation times. Control values were averaged on all the incubation times. Statistical significance levels are indicated as * ($p<0.05$); (b) Confocal microscopy images of PA1 and NF-PA1 samples on J774 cell line at growing incubation times after nuclei staining

Fig. 6. Schematic drawing of sodium taurocholate/mannopyranoside blend arranged on lipid matrix surface

ACCEPTED MANUSCRIPT

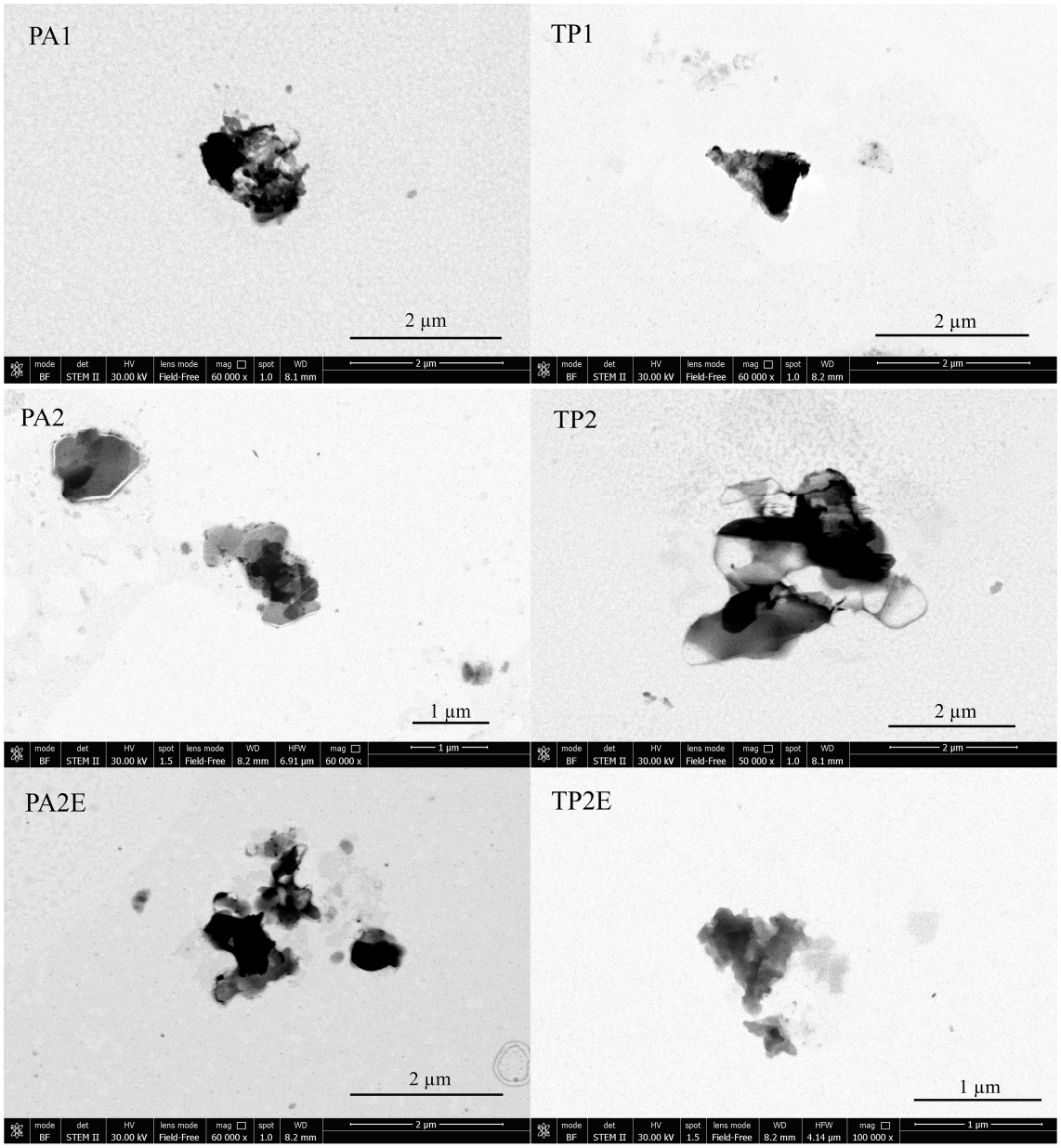

ACCEPTED MANUSCRIPT

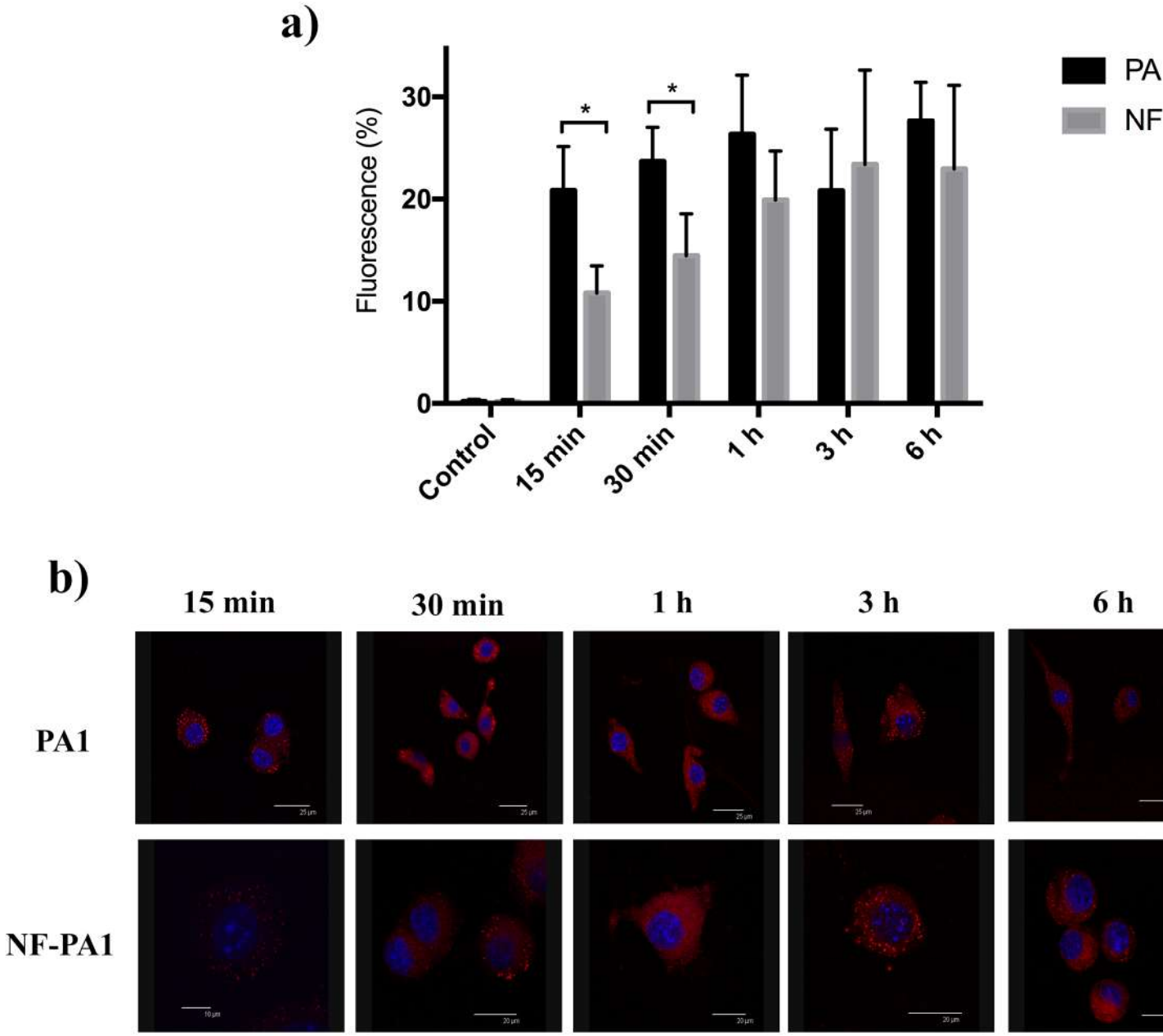

935

ACCEPTED MANUSCRIPT

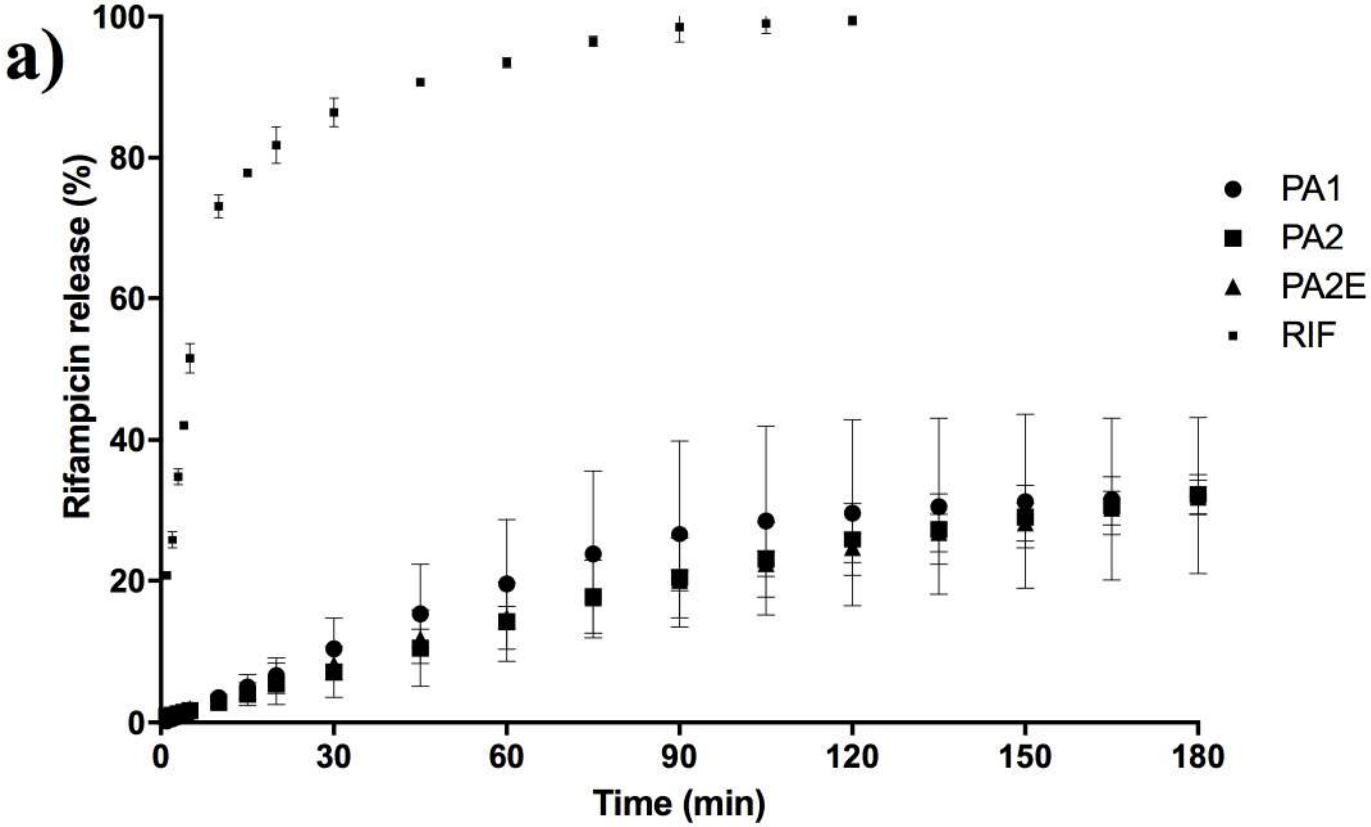

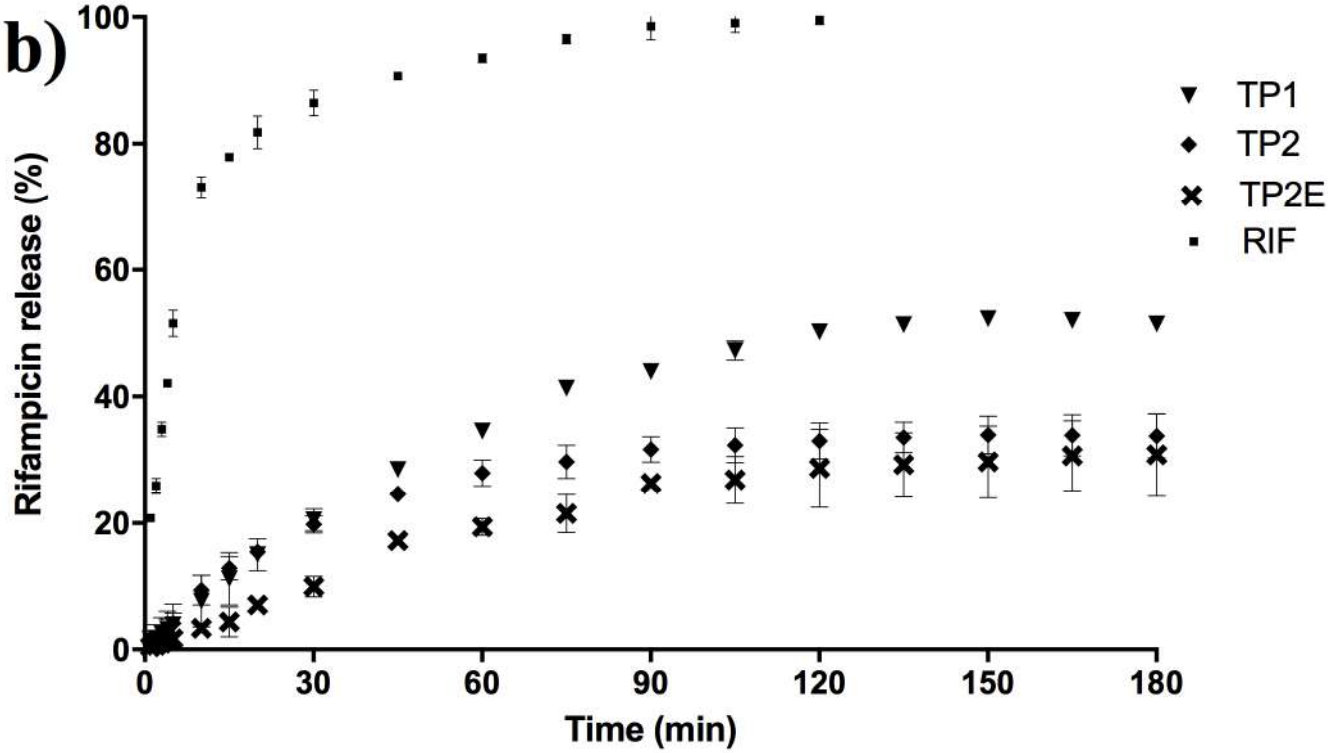

ACCEPTED MANUSCRIPT

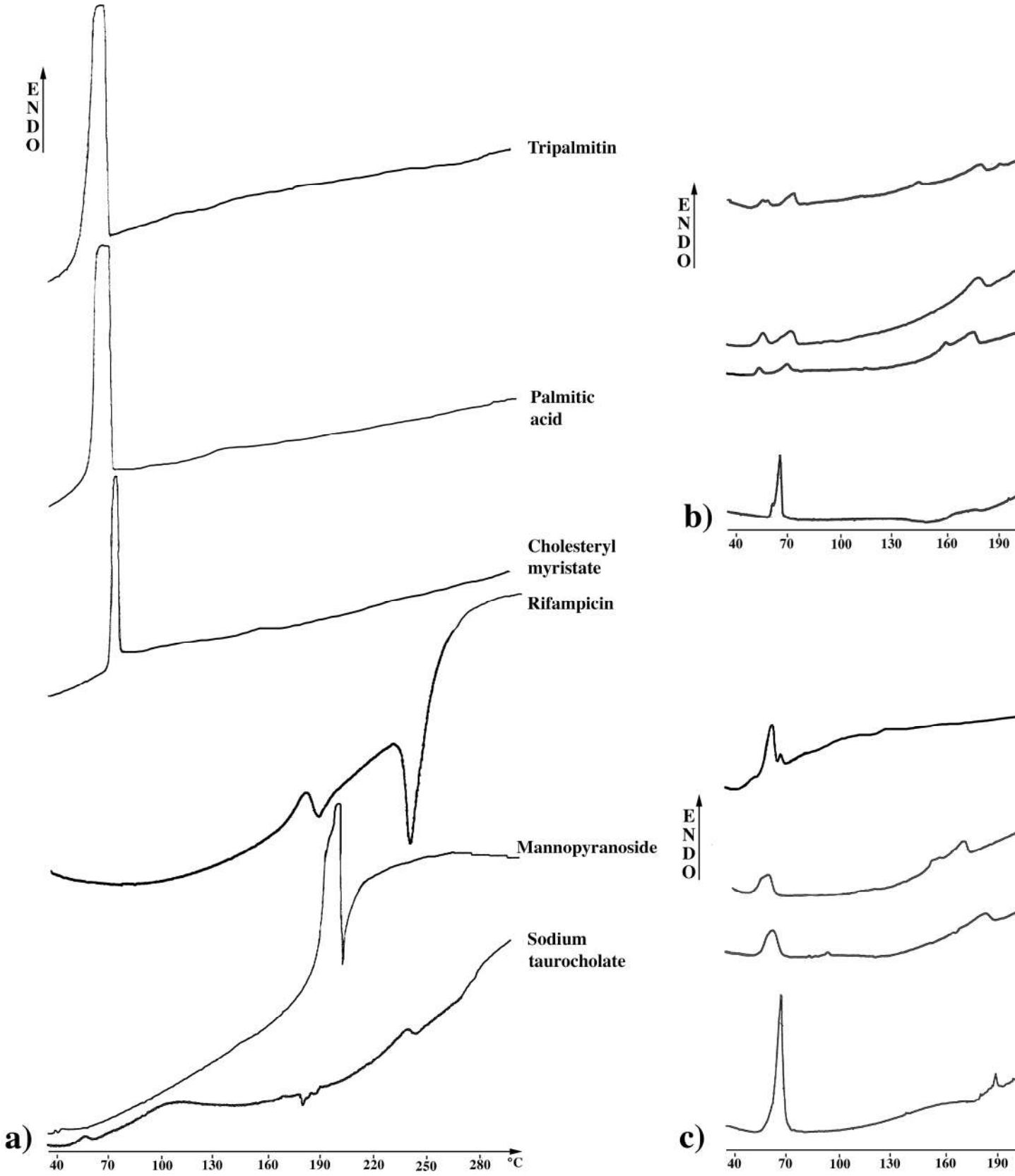

ACCEPTED MANUSCRIPT

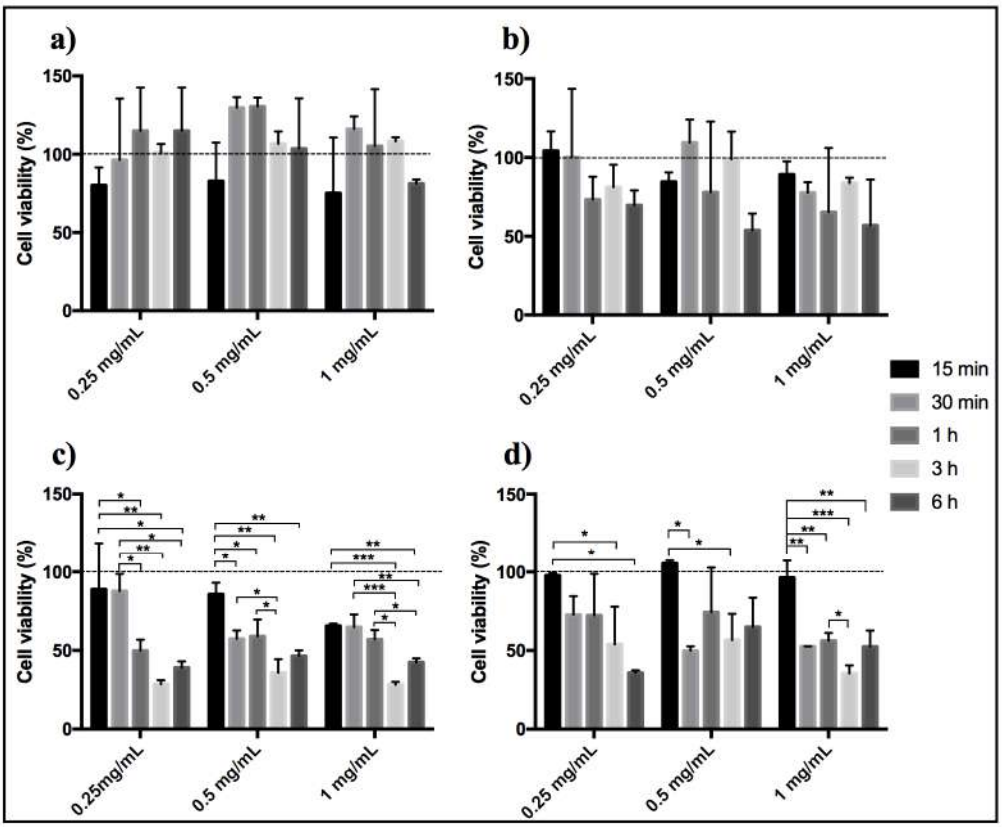

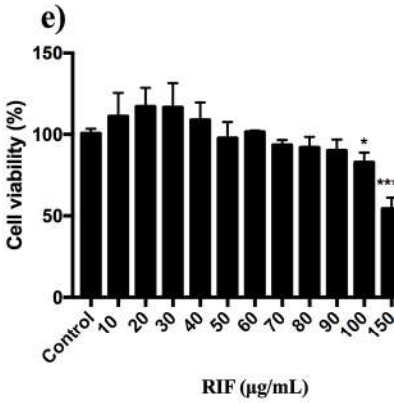
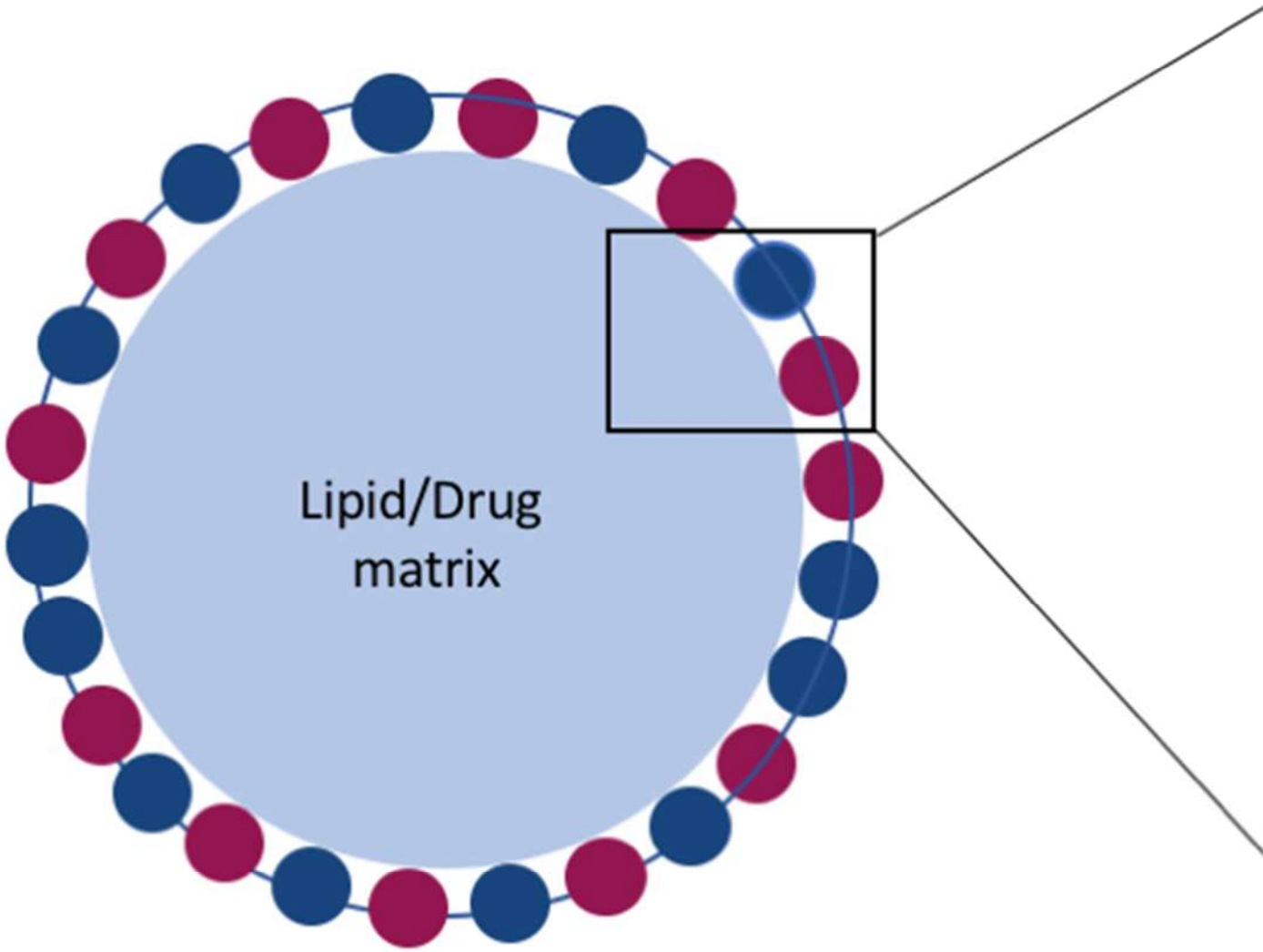
ACCEPTED MANUSCRIPT